Reprogramming of rabbit induced pluripotent stem cells toward epiblast and chimeric competency using Krüppel-like factors

Yann Tapponnier, Marielle Afanassieff, Irène Aksoy, Maxime Aubry, Anaïs Moulin, Lucas Medjani, Wilhelm Bouchereau, Chloé Mayère, Pierre Osteil, Jazmine Nurse-Francis, et al.

Stem Cell Research 24 (2017) 106–117

Contents lists available at ScienceDirect

Stem Cell Research

journal homepage: www.elsevier.com/locate/scr

Reprogramming of rabbit induced pluripotent stem cells toward epiblast and chimeric competency using Krüppel-like factors

Yann Tapponnier [a,1], Marielle Afanassieff [a,*,1], Irène Aksoy [a], Maxime Aubry [a], Anaïs Moulin [a], Lucas Medjani [a], Wilhelm Bouchereau [a], Chloé Mayère [a], Pierre Osteil [a], Jazmine Nurse-Francis [a], Ioannis Oikonomakos [a], Thierry Joly [b,c], Luc Jouneau [d], Catherine Archilla [d], Barbara Schmaltz-Panneau [d], Nathalie Peynot [d], Harmonie Barasc [e,f], Alain Pinton [e,f], Jérome Lecardonnel [g], Elen Gocza [h], Nathalie Beaujean [a], Véronique Duranthon [d], Pierre Savatier [a,*]

[a] Univ Lyon, Université Lyon 1, Inserm, Stem Cell and Brain Research Institute U1208, INRA USC 1361, 69500 Bron, France
[b] ISARA-Lyon, F-69007 Lyon, France
[c] VetAgroSup, UPSP ICE, F-69280 Marcy l'Etoile, France
[d] UMR BDR, INRA, ENVA, Université Paris Saclay, 78350 Jouy-en-Josas, France
[e] INRA, UMR 444, Génétique Cellulaire, F-31076 Toulouse, France
[f] ENVT, F-31076 Toulouse, France
[g] GABI, INRA, AgroParisTech, Université Paris-Saclay, 78350 Jouy-en-Josas, France
[h] Agricultural Biotechnology Institute, H-2100 Gödöllo, Hungary

ARTICLE INFO

Article history:
Received 25 May 2017
Received in revised form 24 August 2017
Accepted 1 September 2017
Available online 05 September 2017

Keywords:
Induced pluripotent stem cells
Rabbit
Krüppel-like factors
Transcriptome
Reprogramming
Embryo

ABSTRACT

Rabbit induced pluripotent stem cells (rbiPSCs) possess the characteristic features of primed pluripotency as defined in rodents and primates. In the present study, we reprogrammed rbiPSCs using human Krüppel-like factors (KLFs) 2 and 4 and cultured them in a medium supplemented with fetal calf serum and leukemia inhibitory factor. These cells (designated rbEKA) were propagated by enzymatic dissociation for at least 30 passages, during which they maintained a normal karyotype. This new culturing protocol resulted in transcriptional and epigenetic reconfiguration, as substantiated by the expression of transcription factors and the presence of histone modifications associated with naïve pluripotency. Furthermore, microarray analysis of rbiPSCs, rbEKA cells, rabbit ICM cells, and rabbit epiblast showed that the global gene expression profile of the reprogrammed rbiPSCs was more similar to that of rabbit ICM and epiblast cells. Injection of rbEKA cells into 8-cell stage rabbit embryos resulted in extensive colonization of ICM in 9% early-blastocysts (E3.5), epiblast in 10% mid-blastocysts (E4.5), and embryonic disk in 1.4% pre-gastrulae (E6). Thus, these results indicate that KLF2 and KLF4 triggered the conversion of rbiPSCs into epiblast-like, embryo colonization-competent PSCs. Our results highlight some of the requirements to achieve bona fide chimeric competency.

1. Introduction

Pluripotent stem cells (PSCs) exist in two distinct states: naïve or ground state of pluripotency (e.g., mouse embryonic stem cells [mESCs] generated from E4.5 epiblast of blastocyst (Boroviak et al., 2014)), and primed state of pluripotency e.g., mouse epiblast stem cells [mEpiSCs] generated from E6–E7.5 epiblast of early post-implantation embryos (Brons et al., 2007; Nichols and Smith, 2009; Tesar et al., 2007). mESCs and mEpiSCs show many differences, both in terms of molecular characteristics and functional properties (Nichols and Smith, 2009). In particular, mEpiSCs, unlike mESCs, cannot create somatic and germ line chimeras after injection into blastocysts (Brons et al., 2007; Tesar et al., 2007). mEpiSCs can be converted to mESCs by enforced expression of genes such as *Klf2*, *Klf4*, *Nanog*, *STAT3* and *Nr5a2* (Guo and Smith, 2010; Guo et al., 2009) (Hall et al., 2009; Silva et al., 2009; Yang et al., 2010), or by inhibiting CK1, MEK and SMAD2 activity and enhancing WNT activity (Illich et al., 2016). The reverted ESCs acquired the characteristics of naïve pluripotency, including transcriptome and epigenome reconfiguration and, when tested, the capacity to make germline chimeras.

PSCs derived from humans and non-human primates (NHPs) exhibit most of the defining features of primed pluripotency (Nichols and Smith, 2009; Vallier et al., 2005; Wianny et al., 2008), including the

* Corresponding authors at: Stem Cell and Brain Institute, INSERM U1208, 18 Avenue du Doyen Lépine, F-69675 Bron Cedex, France.
E-mail addresses: marielle.afanassieff@inserm.fr (M. Afanassieff), pierre.savatier@inserm.fr (P. Savatier).
[1] Equal contributions.

http://dx.doi.org/10.1016/j.scr.2017.09.001

inability to colonize pre-implantation embryos and produce somatic chimeras (Tachibana et al., 2012). Induced pluripotent stem cells (iPSCs) derived from humans and NHPs also exhibit primed pluripotency-like characteristics. Several studies have reported on the reversion of conventional human ESCs and iPSCs to naïve-like pluripotency using different combinations of transcription factors (KLF2, NANOG, and STAT3), growth factors (LIF, Activin A, and FGF2), and chemical inhibitors of various kinases (ROCK, BRAF, $p38^{MAPK}$, GSK3, MEK1/2, SRC, and JNK). The reverted cells, known variously as NHSM (Gafni et al., 2013), 3iL (Chan et al., 2013), Reset (Takashima et al., 2014), 6i/L/A (Theunissen et al., 2014) and TL2i (Chen et al., 2015a), display some characteristic features of naïve pluripotent rodent stem cells, including reconfigured transcriptome and epigenome, alterations in mitochondrial respiration (Takashima et al., 2014), loss of FGF2 and ERK dependency (Chen et al., 2015a; Takashima et al., 2014), and gain of LIF/STAT3 dependency (Chan et al., 2013; Chen et al., 2015a; Takashima et al., 2014). Reversion of cynomolgus macaque ESCs to naïve-like pluripotency has also been reported (Chen et al., 2015b). When introduced into host macaque embryos, these reverted cells seem capable of colonizing the epiblast and differentiating into cells characteristic of the three germ layers in the fetus. However, the frequency of chimerism is low, possibly because very few cells have truly acquired a naïve state. It is also possible that these rare cells have a weak competitive edge against the host cells in contributing to tissue differentiation.

Rabbit (*Oryctolagus cuniculus*) PSCs exhibit the characteristic features of primed pluripotency. They are dependent on FGF2 signaling and TGFβ family receptors for self-renewal (Honda et al., 2009; Osteil et al., 2013; Wang et al., 2008; Wang et al., 2006). Previously, we have shown that they also lack chimeric competency (Osteil et al., 2016; Osteil et al., 2013). In one of those studies, we compared rbESCs with rabbit iPSCs (rbiPSCs) and showed that rbiPSCs spontaneously exhibited some features of naïve pluripotency, including the activity of the distal enhancer of mouse *Oct4*, permissiveness to single-cell dissociation, and high clonogenicity (Osteil et al., 2013).

In the present study, we explored the conditions for reprogramming rbiPSCs into PSCs with molecular and functional properties more akin to the rabbit epiblast. To that end, we overexpressed both KLF2 and KLF4 in the rbiPSCs, and subsequently adapted the cells to propagation in a medium supplemented with LIF and serum. We then explored the transcriptomic and epigenomic reconfiguration, and asked whether the reprogrammed cells acquired the capability to participate in the formation and expansion of the rabbit epiblast.

2. Material and methods

Full details of the experimental procedure are included in Supplemental Experimental Procedures.

2.1. Reprogramming of B19-EOS iPS cells with human Klf2 and Klf4

B19-EOS cells were produced by somatic cell reprogramming of adult rabbit fibroblasts with the human transcription factors OCT4, SOX2, c-MYC, and KLF4, followed by infection with a lentiviral vector, L-SIN-EOS-C(3)-EiP (EOS) (Hotta et al., 2009), and subsequent selection of EOS-expressing cells using puromycin (Osteil et al., 2013). In the *EOS* vector, the GFP and puromycin resistance genes are under the transcriptional control of a minimal early transposon promoter and trimer of CR4 enhancer of mouse *Oct4*. The CR4 enhancer overlaps a distal enhancer whose activity is associated with naïve-like pluripotency (Yeom et al., 1996). In the present study, the B19-EOS cells were transfected with the *pGG137-hK2-2A-hK4* vector, which is a PiggyBac vector expressing human *KLF2* and *KLF4*. Three clones showing low, medium, and high expression of KLF2 and KLF4 were selected. These clones were designated as rabbit Enhanced KLF Activity (rbEKA)-low (low KLF expressor), rbEKA-mid (mid KLF expressor), and rbEKA-high (high KLF expressor).

2.2. Isolation of ICM and epiblast

Early-blastocysts (E4) were collected 96 h after artificial insemination and incubated in 5 mg/ml pronase at room temperature to remove the zona pellucida and mucin coat. The ICM was separated from the trophectoderm by immunosurgery followed by gentle pipetting with a glass pipette. To prepare the epiblasts, expanded blastocysts (E6) were collected 147 h after artificial insemination and placed in FHM medium (Millipore). The zona pellucida was mechanically removed. The embryo was opened and flattened on a plastic dish to expose the embryoblast. The hypoblast was first dissociated by careful scratching with a glass needle, and the epiblast was then separated from the trophoblast with a microscalpel.

2.3. Microarray analysis

We used a customized rabbit microarray containing 62,976 probes (platform GPL16709) (Jacquier et al., 2015). Forty ICMs and 10 epiblasts were pooled prior to RNA extraction. For hybridization, cyanine-3 (Cy3)-labeled cRNAs were prepared from 20 ng RNA (ICM and epiblast samples) and 200 ng RNA (cell lines) by using One-Color Microarray-Based Gene Expression Analysis Low Input Quick Amp Labelling Kit (Agilent Technologies). To verify that the use of a 10-fold lower quantity of RNA from embryo samples as compared with cell lines, did not significantly skew the outcome of the hybridization experiment, test hybridization using 20 ng and 200 ng of RNA from cell lines was performed, and the intensity of the hybridization signals was compared between both conditions. None of the 62,976 probes showed a statistically significant difference in signal intensity between the two RNA quantities (BH corrected p-value < 0.05, ratio > 2), validating our experimental paradigm. For all samples, 0.6 μg Cy3-labeled cRNA (specific activity, >6.0 pmol Cy3/μg of cRNA) was used for hybridization of the microarray. After hybridization, the scanned images were analyzed using Feature Extraction Software (7.10.3.1; Agilent Technologies). Data were normalized using intra-array median subtraction and $\log_2$ transformation. Differential analysis was performed using Limma R package (http://www.r-project.org), and JADE R package was used to compute independent component analyses (ICA).

2.4. Single-cell gene expression analysis with qRT-PCR

Real-time PCR (qPCR) was performed using the CellsDirect™ One-Step qRT-PCR kit (ThermoFisher) coupled with the StepOnePlus real-time PCR system and Fast SBYR® Green Master Mix (Applied Biosystems). Expression of the target genes was normalized to that of the rabbit TATA-box binding protein (*Tbp*) and *Gapdh* genes. For single-cell qPCR, cells were dissociated using trypsin, manually separated. Reverse transcription and specific target amplification were performed using the SuperScript III/RT Platinum Taq mix provided in the kit. The pre-amplified products were subsequently analyzed with Universal PCR TaqMan Master Mix (Applied Biosystems) and coupled with a DNA Binding Dye Sample Loading Reagent (Fluidigm) and Evagreen (Biotium 31000) in 96.96 Dynamic Arrays on a BioMark System.

2.5. miRNA quantification

Mature miRNA quantification was performed via a two-step protocol including reverse transcription with miRNA-specific primers using a TaqMan MicroRNA Reverse Transcription Kit, followed by quantitative real-time PCR with TaqMan MicroRNA Assays-TM. Expression of the target miRNAs was normalized to the housekeeping miRNAs *ocu-miR-191* and *ocu-miR-423*.

2.6. Cell microinjection, embryo culture, and transfer to surrogates

8-cell-stage embryos (E1.5) were flushed from explanted oviducts and cultured in RDH medium. Cells were dissociated into single-cell suspensions, and 5–10 cells were microinjected under the zona pellucida of 8-cell stage rabbit embryos (E1.5). After 48 h of in vitro culture in RDH medium, early blastocyst stage embryos (E3.5) were treated with pronase to digest the mucus coat. They were further cultured in RDH medium for 24 h until they reached the mid-blastocyst stage (E4.5) prior to immunostaining with AF488-conjugated rabbit anti-GFP antibody or Anti-Oct4 antibody. For embryo transfer, the surrogates were prepared by injecting 1.6 μg of buserelin acetate (Receptal®, Intervet) intramuscularly. Eight-cell stage embryos (6–8) were transferred to each oviduct of the recipient by performing laparoscopy (Besenfelder et al., 1998). Five days after the transfer, embryos in the pre-implantation stage (E6) were recovered by flushing the explanted uterine horns and were fixed in 2% PFA prior to immunostaining. Fetuses were recovered at E10, examined for dsRed fluorescence, and subsequently processed for extraction of genomic DNA and PCR.

3. Results

3.1. Growth properties of B19-EOS rbiPSCs overexpressing KLF2 and KLF4

Three clones were generated from B19-EOS iPS cells, designated as rabbit Enhanced KLF Activity (rbEKA)-low (low KLF expressor), rbEKA-mid (mid KLF expressor), and rbEKA-high (high KLF expressor). They show low, medium, and high expression of KLF2 and KLF4 using qRT-PCR with human-specific primers, and by immunolabeling and immunoblotting with human-specific antibodies (Fig. 1A,B). These three clones exhibited a non-uniform expression of GFP, suggesting heterogeneous activity of the distal enhancer of *Oct4* and, therefore, variable cell states. The GFP and Oct4 were co-expressed in most cells (Fig. 1C). A gradual loss of both GFP and Oct4 expression was observed during differentiation (Supplementary Fig. S1). The rbEKA cell lines were dissociated with trypsin and were propagated for >30 passages. They exhibited the typical morphology of rabbit iPSCs (Supplementary Fig. S2A). Conventional Giemsa staining showed large number of cells with a normal chromosome number for all the 3 cell lines (44 in >70 metaphase

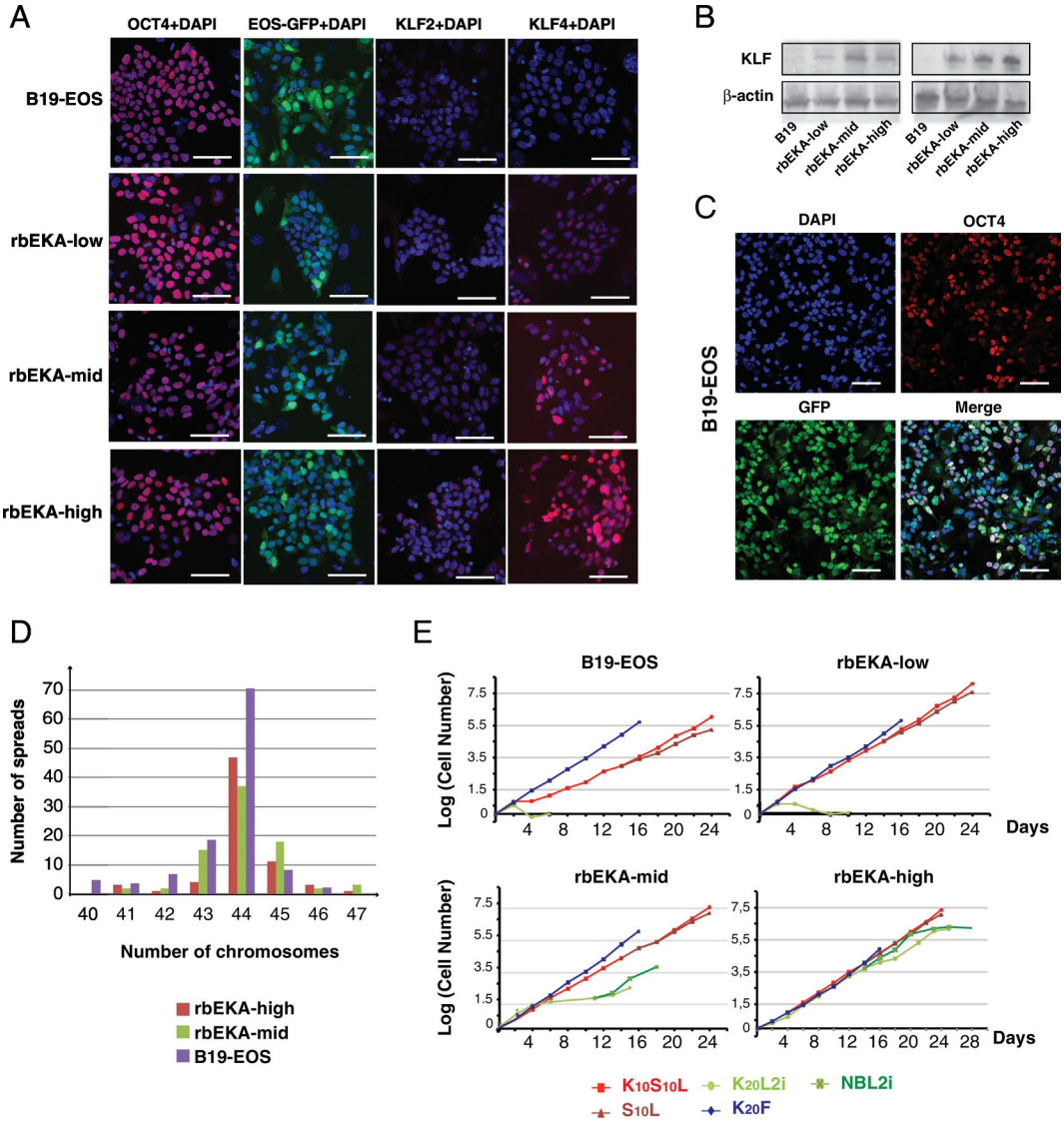

Fig. 1. Propagation of reprogrammed B19-EOS cells. (A) GFP fluorescence associated with EOS expression, and immunolabeling of KLF2 and KLF4 in B19-EOS, rbEKA-low, rbEKA-mid, and rbEKA-high cells. Nucleus is labeled with DAPI (scale bar = 50 μm). (B) Detection of KLF2, KLF4 and β-actin by immunoblotting in B19, rbEKA-low, rbEKA-mid, and rbEKA-high cells. (C) GFP fluorescence associated with *EOS* expression, and immunolabeling of Oct4 in B19-EOS cells. Nucleus is labeled with DAPI (scale bar = 50 μm). (D) Histogram showing the distribution of chromosome numbers in B19-EOS (passage 34), rbEKA-mid (passage 24), and rbEKA-high (passage 28) cells. (E) Growth curves for B19-EOS, rbEKA-low, rbEKA-mid, and rbEKA-high cells after propagation for 7–14 days in $K_{20}F$ (20% KOSR + 10 ng/ml FGF2), $K_{10}S_{10}L$ (10% KOSR + 10% FCS + 1000 U/ml LIF), $S_{10}L$ (10% FCS + 1000 U/ml LIF), $K_{20}L2i$ (20% KOSR + 1000 U/ml LIF + 3 μM CHIR99021 + 1 μM PD0325901), and NBL2i (N2B27 + 1000 U/ml LIF + 3 μM CHIR99021 + 1 μM PD0325901) media.

spreads analyzed; Fig. 1D). The cells were karyotyped using G-banding, and normal chromosome complements (42XX) were observed in the metaphase spreads (Supplementary Fig. S2B).

The three rbEKA cell lines and control B19-EOS cells were passaged 7 times in a medium supplemented with (i) 20% KOSR and 10 ng/ml FGF2 ($K_{20}F$ medium), (ii) 10% KOSR +10% fetal calf serum (FCS) + 1000 U/ml LIF ($K_{10}S_{10}L$ medium), and (iii) 20% KOSR + 1000 U/ml LIF + 3 μM CHIR99021 + 1 μM PD0325901 ($K_{20}L2i$ medium), all on feeder cells (Fig. 1E and Supplementary Fig. S3). All the four cell lines showed similar growth rates when propagated in the $K_{20}F$ medium. However, the three rbEKA cell lines grew faster than the control B19-EOS cells in $K_{10}S_{10}L$ medium. In $K_{20}L2i$, the B19-EOS and rbEKA-low cells failed to expand completely, the rbEKA-mid cells expanded only for 6 passages (15 days) before showing growth arrest, and the rbEKA-high cells expanded for 12 passages (24 days) before showing growth arrest. After propagation in $K_{20}L2i$ for 7 passages (14 days), the rbEKA-mid and rbEKA-high cells were transferred to a neurobasal medium (N2B27) supplemented with 1000 U/ml LIF + 3 μM CHIR99021 + 1 μM PD0325901 (NBL2i medium). The rbEKA-mid cells stopped proliferating within 6 days, while the rbEKA-high cells proliferated for 5 passages (10 days), after which they also showed growth arrest. These data indicate that robust expression of KLF2 and KLF4 was associated with transient growth in the presence of MEK and GSK3β inhibitors. After propagation in $K_{10}S_{10}L$ medium for 14 days, the four cell lines were transferred to a medium supplemented with 10% FCS + 1000 U/ml LIF (designated as $S_{10}L$ medium). The three rbEKA cell lines grew faster than B19-EOS cells in $S_{10}L$. They could be expanded for 40 passages (80 days) with no significant change in growth rate and morphology. This suggests that robust expression of KLF2 and KLF4 was associated with long-term growth in a medium supplemented with FCS and LIF and mid-term growth in 2i + LIF condition.

3.2. Pluripotency gene and miRNA expression profiling

We examined the mRNA expression of rabbit homologs of the 21 mouse genes shown in Fig. 2A a by using RT-qPCR analysis in the three rbEKA cell lines and control cells, during propagation in the $K_{20}F$ medium for 7 passages, $K_{10}S_{10}L$ for 11 passages, and $S_{10}L$ for 4 passages. Most of these genes are commonly used to characterize naïve versus primed pluripotency in mouse cells (Bao et al., 2009; Boroviak et al., 2015; Hanna et al., 2010; Tang et al., 2010; Tesar et al., 2007). PCA of gene dispersion, which was graphically represented in a trigonometric circle (Fig. 2Aa), highlighted a representative cluster of 12 genes (*Nanog*, *Rex1*, *Esrrb*, *Dppa2*, *Dppa5*, *Tbx3*, *Dazl*, *Fgf4*, *Piwil2*, *Cdh1*, *Otx2*, and *Lefty2*), which explained most of the variability observed in the samples. We compared gene expression profiles of the four cell lines in all the culture media ($K_{20}F$, $K_{10}S_{10}L$, and $S_{10}L$). PCA showed that these cell lines formed two distinct clusters, with B19-EOS (control) and rbEKA-low cell lines in one cluster and rbEKA-mid and rbEKA-high cell lines in the other (Fig. 2Ab). Both rbEKA-mid and rbEKA-high cell lines showed higher expression of *Nanog*, *Dppa2* and *Dppa5*, and mouse naïve pluripotency markers *Rex1*, *Dazl*, and *Piwil2* than that in B19-EOS and rbEKA-low (Supplementary Fig. S4). In addition to these six genes, rbEKA-mid cells showed increased expression of the naïve pluripotency markers *Esrrb* and *Tbx3*, and rbEKA-high cells showed increased expression of the mouse naïve pluripotency marker *Fgf4*. By using the same compendium, we then compared gene expression profiles of all the cell lines in the three media ($K_{20}F$, $K_{10}S_{10}L$, and $S_{10}L$). PCA showed that the cells propagating in $K_{10}S_{10}L$ and $S_{10}L$ media were clustered together (Fig. 2Ac). High mRNA expression was observed for *Esrrb*, *Dppa5*, *Tbx3*, *Dazl, Fgf4*, *Cdx2* and *Otx2* after propagation in the $K_{10}S_{10}L$ and $S_{10}L$ media (Supplementary Fig. S5). High mRNA expression was also observed for *Rex1* in $S_{10}L$. These results indicate that KLF expression and media composition altered the pluripotency gene expression pattern of rbiPSCs by activating the expression of genes associated with naïve pluripotency in mice.

Then, we next examined the cell lines that showed the highest similarity to ICM cells by comparing the pluripotency gene expression profiles of rbEKA-high and rbEKA-mid cell lines propagated in $S_{10}L$ with those of non-reprogrammed B19-EOS cells and ICM cells in the early-blastocyst stage (E3.5). We observed that rbEKA-high and rbEKA-mid cells cultured in $S_{10}L$ were clustered closer to the ICM than B19-EOS cells cultured in $K_{20}F$ (Supplementary Fig. S6). Graphical representation of gene dispersion in a trigonometric circle highlighted two anti-correlated clusters, which explained most of the variability observed between the samples. The genes in cluster 1 included *Nanog*, *Rex1*, *Esrrb*, *Dppa2*, *Dppa5*, *Tbx3*, *Dazl*, *Fgf4*, *Cdh1*, and *Otx2*. They were characterized by lower mRNA levels in the B19-EOS cells compared with the E3.5-stage ICM (relative expression normalized to ICM < 1). The mRNA levels increased dramatically after conversion to rbEKA state, thus approaching the levels measured in the ICM. Genes in cluster two included *Cldn6*, *Fbxo15*, *Pecam1*, *Cdh2*, *Nr0b1* (*Dax1*), and *Gbx2*. They were characterized by higher mRNA levels in the B19-EOS cells compared with the ICM (relative expression normalized to ICM > 1). The RNA levels decreased dramatically after reprogramming to rbEKA state, thus approaching the levels measured in the E3.5-stage ICM. The proximity of rbEKA-mid and rbEKA-high cell lines (propagated in the $S_{10}L$ media) to ICM was confirmed after analyzing 22 additional genes (Fig. 2B). This analysis included *Klf4*, *Klf5*, *Klf17*, *Dppa3* (*Stella*), *Dppa4*, *Epcam1*, *Lin28A*, and *Esrrg*, which were upregulated in rbEKA and ICM as compared with B19 cells.

Ocu-miR-294 and *ocu-miR-302* are two miRNA clusters expressed in rabbit pre-implantation embryos. Expression of the *ocu-miR-294* cluster starts at the 1-cell stage and reaches a peak in the ICM of mid-blastocysts (E4.0–E4.5). In contrast, the *ocu-miR-302* cluster is strongly expressed in the epiblast of early gastrulation embryos (E6–E7) (Maraghechi et al., 2013). rbEKA cells cultivated in the $S_{10}L$ media showed a 100-fold increase in the expression of the *ocu-miR-294* cluster, and no alteration in the expression of the *ocu-miR-302* cluster compared with B19-EOS cultivated in the K20F media (Fig. 2C), suggesting that rbEKA cells acquired an ICM-like profile of miRNA expression.

Together, these results indicated that forced expression of KLF2 and KLF4 in conjunction with propagation in a medium supplemented with FCS and LIF allowed rbiPSCs to acquire a pluripotency gene expression profile more akin to that of rabbit ICM cells.

3.3. Benchmarking of rbEKA-$S_{10}L$ cells to ICM and epiblast

To determine whether rbEKA-mid and rbEKA-high cells cultivated in the $S_{10}L$ media (hereafter designated rbEKA-mid-$S_{10}L$ and rbEKA-high-$S_{10}L$ cells, respectively) underwent whole transcriptome reconfiguration, we used rabbit-specific gene expression microarray analysis (Schmaltz-Panneau et al., 2014) to analyze the expression of approximately 13,000 genes in B19 and B29 iPSCs (Osteil et al., 2013) and in the B19-EOS, rbEKA-mid-$S_{10}L$, and rbEKA-high-$S_{10}L$ cells. Gene expression profiles of these cells were compared to those of rabbit fibroblasts (RbF), E4-stage ICM, and E6-stage epiblast. Detailed information on the characterization of ICM and epiblast samples is provided in Supplementary Fig. S7. Hierarchical clustering of normalized data showed that all rbEKA-$S_{10}L$ cells (i.e., both rbEKA-mid-$S_{10}L$ and rbEKA-high-$S_{10}L$ cells) were clustered closer to the ICM and epiblast than the original iPSCs (Fig. 3A), which is in accordance with the results of the qRT-PCR analysis. One component of independent component analysis (ICA) corroborated these results by showing two distinct clusters, with the first containing original iPSCs and RbFs and the second containing all the reprogrammed cells (rbEKA-$S_{10}L$) and embryo samples (ICM cells and epiblast; Fig. 3B). Thus, we concluded that rbEKA-$S_{10}L$ cells reconfigured their transcriptome to resemble that of pluripotent cells in pre-implantation embryos. For more insight on the relative proximity of rbEKA-$S_{10}L$ cells with E4-stage ICM and E6-stage epiblast, PCA was performed using transcriptomic array signal values for *Cdx2*, *Cdh1*, *Cdh2*, *Cldn6*, *Cyp1b1, Dax1* [*Nr0b1*], *Dazl*, *Dppa5*, *Esrrb*, *Fbxo15*, *Gbx2*, *Klf4*, *Nanog*,

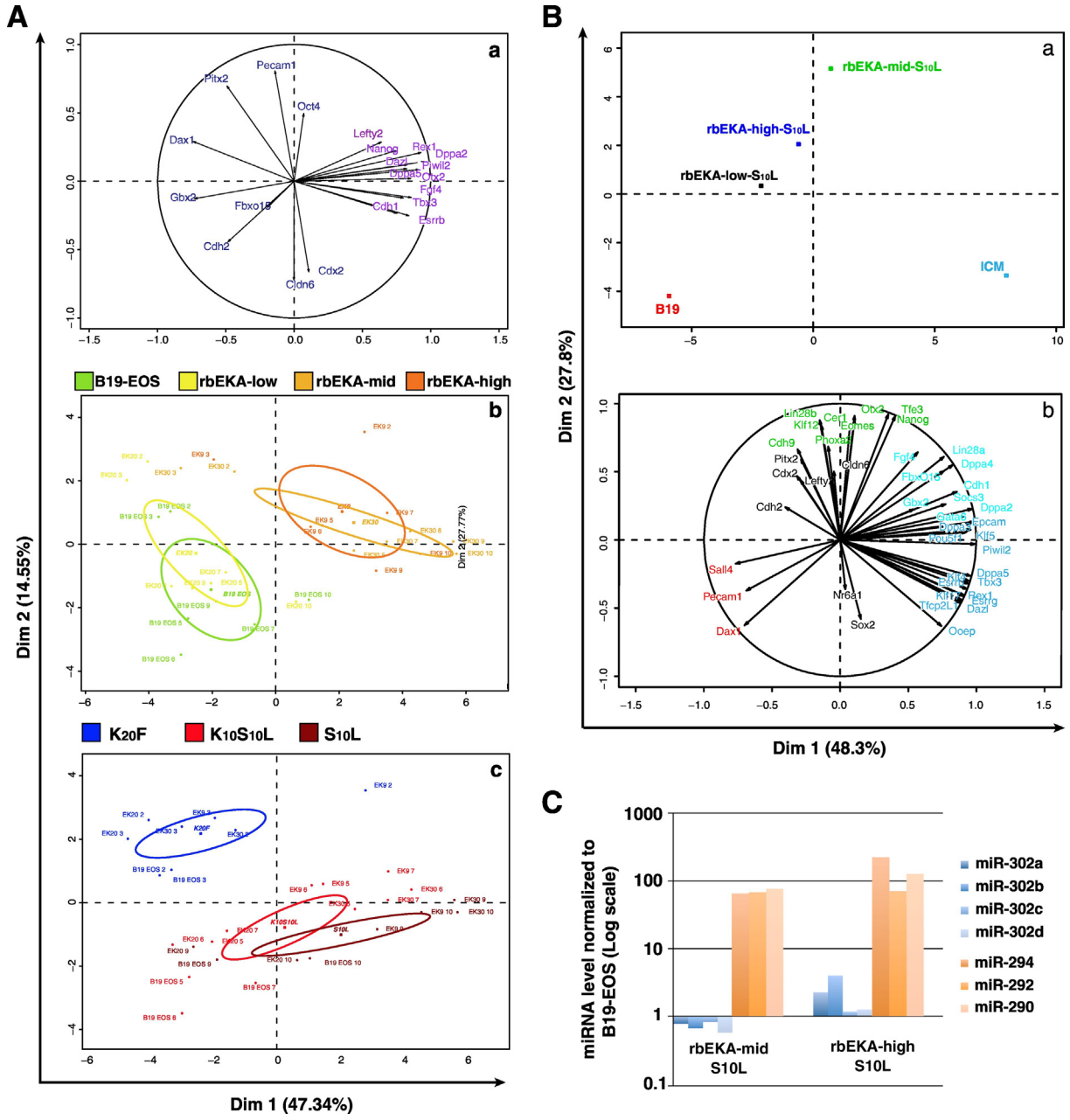

Fig. 2. Pluripotency gene and miRNA expression profiling. (A) Graphical representation of the first two principal components of PCA for B19-EOS, rbEKA-low, rbEKA-mid, and rbEKA-high cells based on the mRNA levels of the 21 selected genes; (upper panel a) trigonometric circle showing the relative contribution of the genes to the variability between all the samples; (mid panel b) plane projection showing clusters based on cell lines; (bottom panel c) plane projection showing clusters based on culture media. (B) Graphical representation of the first two principal components of PCA for B19 cells in $K_{20}F$ medium, rbEKA-low- $S_{10}L$, rbEKA-mid-$S_{10}L$ and rbEKA-high-$S_{10}L$ cells, and ICM cells; (top panel a) plane projection; (bottom panel) b trigonometric circle. (C) Histograms for the expression of pre-implantation embryo-specific *ocu-miR-302* and *ocu-miR-294* clusters relative to the levels of *ocu-miR-191* and *ocu-miR-423* in rbEKA-mid-$S_{10}L$ and rbEKA-high-$S_{10}L$ cells after normalization to expression in B19-EOS.

Oct4 [*Pou5f1*], *Otx2*, *Pecam1*, *PhoxA2*, *Prdm1*, *Tbx3*, and *Tfcp2l1*, and *Zfp42* in B19, B19-EOS, B29, rbEKA-mid-$S_{10}L$, and rbEKA-high-$S_{10}L$ cells (Fig. 3C). The first axis represented 55% of the total variability and was able to distinguish between conventional iPS cells (B19, B19-EOS, B29), rbEKA-$S_{10}L$ cells and epiblast, and ICM samples. The second axis represented 20% of the total variability and was able to distinguish rbEKA-$S_{10}L$ cells and epiblast from ICM. PCA of gene dispersion highlighted 11 genes (*Cdh1, Klf4, Dppa5, Zfp42, Pitx2*, *Esrrb, Tfcp2l1, Dazl, Piwil2*, *Gbx2*, *Nr0b1*, and *Cdh2*), which explained most of the variability observed in the samples (Fig. 3D). Thus, on the basis of the 21 genes examined, rbEKA-$S_{10}L$ cells clustered closer to E6-stage epiblast than to E4-stage ICM.

3.4. Signaling pathways

To gain insights on the signaling pathways involved in self-renewal, rbEKA-mid-$S_{10}L$ and rbEKA-high-$S_{10}L$ cells were propagated for 3 passages in $S_{10}L$ medium lacking LIF, and that supplemented with pharmacological inhibitors of JAK2 (0.5 μM SD1029), FGF receptor (10 μM SU5402), and activin receptor (1 μM SB431542; Fig. 4A,B). We observed that rbEKA-mid-$S_{10}L$ and rbEKA-high-$S_{10}L$ cells grown in the medium lacking LIF showed morphology and growth rate similar to that of control cells. Cells grown in the medium supplemented with JAK2 inhibitor showed slightly reduced growth rate, but undifferentiated morphology. In contrast, rbEKA-mid-$S_{10}L$ and rbEKA-high-$S_{10}L$ cells propagated in a

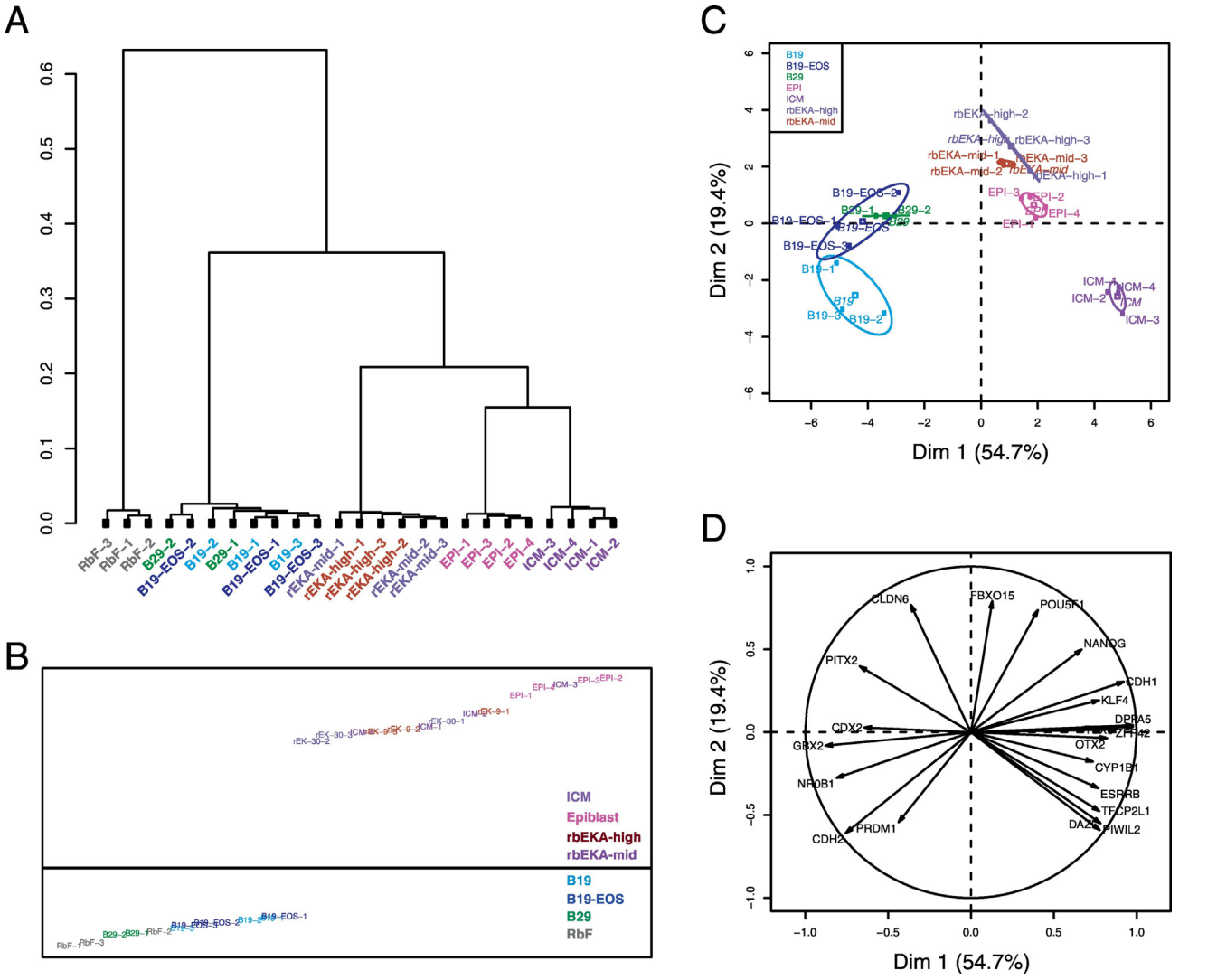

Fig. 3. rbEKA-S_{10}L cells, ICM and epiblast benchmarking. (A) Hierarchical clustering of whole transcriptome data of all cell types (2 or 3 replicates per category) by using Pearson correlation coefficient as a measure of the distance between the samples. (B) Graphical representation of one component of ICA for all the analyzed samples calculated from the transcriptome data. (C) Graphical representation of the two first principal components of PCA calculated from the normalized transcriptome microarray signals for *Cdx2*, *Cdh1*, *Cdh2*, *Cldn6*, *Cyp1b1*, *Dax1* [*Nr0b1*], *Dazl*, *Dppa5*, *Esrrb*, *Fbxo15*, *Gbx2*, *Klf4*, *Nanog*, *Oct4* [*Pou5f1*], *Otx2*, *Pecam1*, *PhoxA2*, *Prdm1*, *Tbx3*, and *Tfcp2l1*, and *Zfp42* in B19, B19-EOS, B29, rbEKA-mid-S_{10}L, rbEKA-high-S_{10}L cells, ICM and epiblast. (D) Trigonometric circle showing the relative contribution of the genes to the variability between all the samples analyzed in C.

medium containing inhibitor of FGF receptor or activin receptor showed differentiated morphology and dramatically reduced growth rate. Cells treated with both the inhibitors stopped multiplying. Propagation of these cells in the presence of FGF and/or activin receptor inhibitors resulted in decreased mRNA expression of *Oct4* and *Nanog*, thus confirming differentiation (Fig. 4C). These results indicated that rbEKA-mid-S_{10}L and rbEKA-high-S_{10}L cells depend on FGF and activin signaling, but not on LIF, for inhibiting differentiation.

3.5. Epigenetic reconfiguration

We then examined four different epigenetic marks, two permissive (H3K14 and H3K9 acetylation) and two repressive (H3K9 trimethylation and DNA 5′-cytosine methylation), in rbEKA-high-S_{10}L cells and compared them with B19-EOS cells to evaluate their epigenetic reconfiguration upon reprogramming. All four epigenetic markers could be detected with the expected nuclear distribution (Fig. 5A). Both histone H3 acetylation marks (H3K9ac and H3K14ac) showed a dispersed punctuated staining. H3K14 acetylation did not significantly differ between B19-EOS and rbEKA-high-S_{10}L cells, and we observed a strong increase in H3K9 acetylation in rbEKA-high-S_{10}L cells, which was confirmed by imaging and quantification ($p < 0.001$). H3K9 trimethylation staining accumulated on heterochromatin clusters dropped in rbEKA-high-S_{10}L cells compared with B19-EOS cells ($p < 0.001$). DNA methylation (diffuse 5MeC staining with perinuclear accumulations) significantly decreased in rbEK-high-S_{10}L cells ($p < 0.001$). This suggests that repressive epigenetic marks tend to decrease and are replaced by permissive ones upon reprogramming. The rbEKA-high-S_{10}L cells adopted a more open chromatin configuration, characteristic of more naïve cells (Smith et al., 2016).

3.6. Integration into ICM and colonization of epiblast

To assess the capability of rbEKA-mid-S_{10}L and rbEKA-high-S_{10}L cells to differentiate into ectoderm, mesoderm, and endoderm cells, they were injected into the testes and kidneys of SCID mice. Both the cell lines formed teratomas containing hair follicles, skin structures, cartilage, muscle, digestive tract, and glandular structures, thus confirming pluripotency (Supplementary Fig. S8). rbEKA-mid-S_{10}L and rbEKA-high-S_{10}L cells were infected with the *pGAE-CAG-dsRed/wpre* lentiviral vector expressing *dsRed* under the control of the ubiquitous CAG promoter. FACS-sorted dsRed-positive cells were further propagated for 6

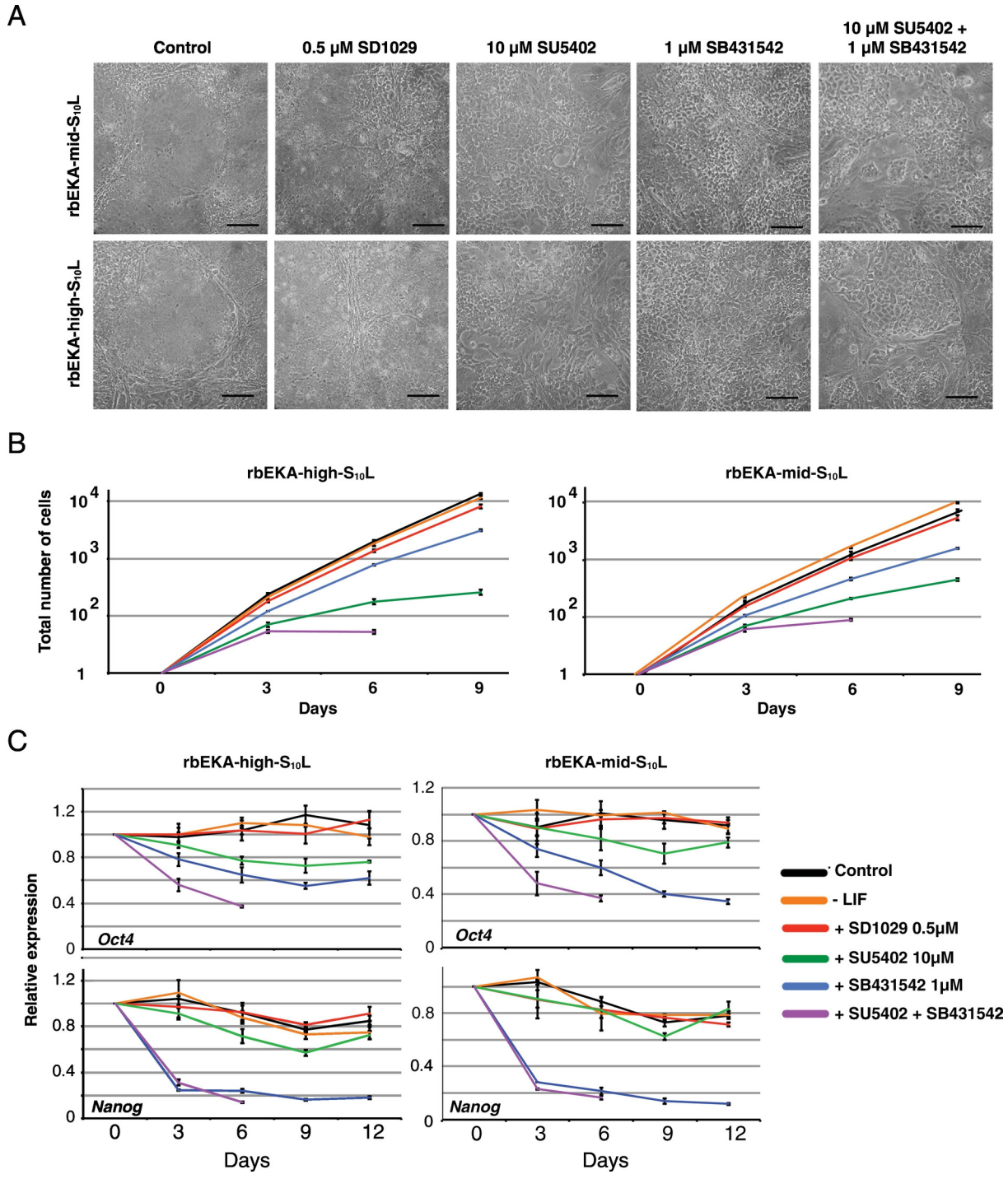

Fig. 4. Signaling pathways. (A) Phase-contrast images of rbEKA-mid-S_{10}L and rbEKA-high-S_{10}L cells after propagation for 12 days in the S_{10}L media (control cells), or supplemented with JAK inhibitor (SD1029), FGFR inhibitor (SU5402), ALK inhibitor (SB431542), and FGFR + ALK inhibitors (scale bar = 50 μm). (B) Growth of rbEKA-mid-S_{10}L and rbEKA-high-S_{10}L cells after propagation for 12 days in the S_{10}L media lacking LIF or supplemented with JAK inhibitor (SD1029), FGFR inhibitor (SU5402), ALK inhibitor (SB431542), and FGFR + ALK inhibitors. (C) Quantitative RT-PCR of *Oct4* and *Nanog* expression in rbEKA-mid-S_{10}L and rbEKA-high-S_{10}L cells after propagation for 12 days in S_{10} L medium lacking LIF or supplemented with JAK inhibitor (SD1029), FGFR inhibitor (SU5402), ALK inhibitor (SB431542), and FGFR + ALK inhibitors (n = 3, mean ± s. d.).

passages to ensure stable expression of the fluorescent marker. Differentiation of rbEKA-mid-S_{10}L-dsRed and rbEKA-high-S_{10}L-dsRed cells into EBs was accompanied with decreased green fluorescence associated with *EOS* expression, decreased *Nanog*, *Oct4*, and *Cdh1* expression, and increased ectodermal (*Nestin* and *Gfap*), mesodermal (*Tbra* and *Flk1*), and endodermal (*Afp* and *Cxcr4*) marker expression (Supplementary Fig. S9). These data further demonstrated the capability of rbEKA-S_{10}L cells to differentiate into ectodermal, mesodermal, and endodermal cells. In order to evaluate the possible heterogeneity of the rbEKA-high-S_{10}L cell population prior to micro-injection into embryos, the expression of 36 genes was analyzed in 41 cells by single-cell quantitative PCR. A strong heterogeneity in mRNA level was observed with markers of the naïve state defined in mice such as *Cdh1*, *Cdh9*, *Fgf4*, *Klf12*, *Tbx3*, *Klf17*, *Fbxo15*, *Gbx2*, and *Esrrb*, and with *Sox2*, *Lin28*, *Nanog*, and *Zscan4* (Supplementary Fig. S10).

We then investigated the capacity of rbEKA-S_{10}L and rbEKA-S_{10}L-dsRed cells to integrate into the ICM of rabbit blastocysts (Fig. 6A). Given the heterogeneity of the rbEKA-high-S_{10}L cell population, as

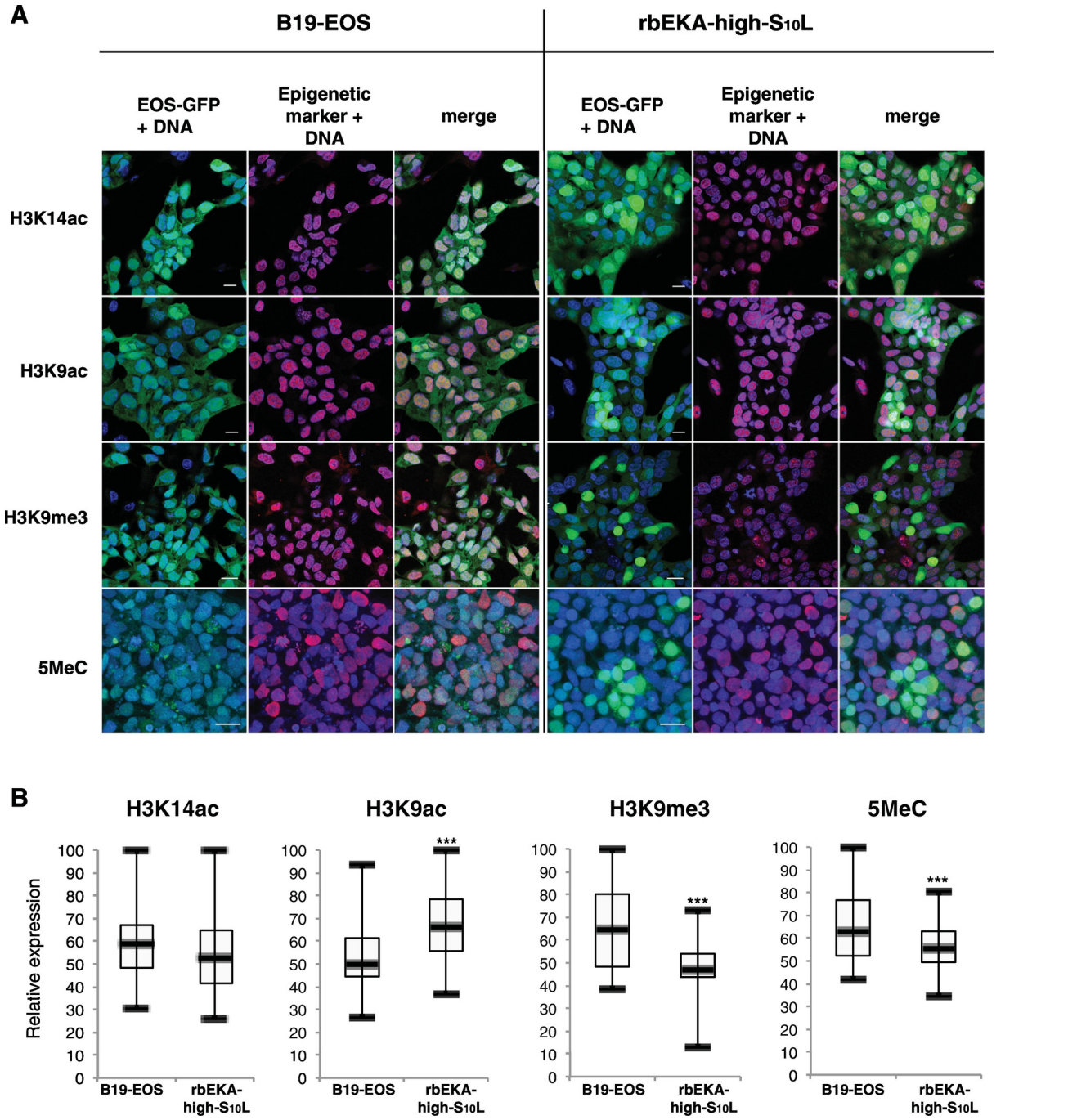

Fig. 5. Epigenetic reconfiguration. Immunolabeling of B19-EOS and rbEKA-high-S_{10}L cells (GFP expression in green) with various epigenetic markers (red), either permissive (H3K14ac and H3K9ac) or repressive (H3K9me3 and 5MeC), and DNA counterstaining (blue). (A) Confocal single z-sections (scale bars = 20 μm). (B) Boxplot representation of the corresponding fluorescent intensities quantifications.

substantiated by single-cell PCR, 5–10 B19-EOS, rbEKA-mid-S_{10}L, and rbEKA-high-S_{10}L cells were injected under the zona pellucida of 8-cell stage rabbit embryos (54, 52, and 62 recipient embryos, respectively) and were cultured for 2 days to the early-blastocyst stage (E3.5). GFP-positive cells were not detected in the ICM of blastocysts injected with B19-EOS cells. In contrast, injection of rbEKA-mid-S_{10}L and rbEKA-high-S_{10}L cells respectively produced 4 (8%) and 6 (10%) embryos with GFP-positive cells in the ICM (Fig. 6B, and Supplementary Table S1). In the second step, rbEKA-S_{10}L and rbEKA-S_{10}L-dsRed cells were used to assess the capability of the reprogrammed cells to colonize the epiblast at the mid-blastocyst stage (E4.5). For this, 5–10 B19-EOS, rbEKA-mid-S_{10}L, rbEKA-mid-S_{10}L-dsRed, rbEKA-high-S_{10}L, and rbEKA-high-S_{10}L-dsRed cells were injected under the zona pellucida of 8-cell stage rabbit embryos (33, 316, and 347 recipient embryos, respectively). The injected embryos were cultured for 2 days until they reached the early-blastocyst stage (E3.5). The mucus coat and zona pellucida were removed, and the embryos were cultured further for 2 days. We found that 139 (25%) E4.5-mid blastocysts contained dsRed- and/or GFP-positive cells after injection of rbEKA-S_{10}L or rbEKA-S_{10}L-dsRed cells. Almost half of these embryos showed extensive colonization of the epiblast (Fig. 6C–E, Supplementary Table S1). rbEKA-high-S_{10}L cells showed colonization at 11, 16, 20, 25, 35 and 40 passages, and rbEKA-mid-S_{10}L cells showed colonization at 15, 16, 24, 28, 30 and 40 passages (Fig. 6F, and Supplementary Table S1). Furthermore, rbEKA-high-S_{10}L cells, which expressed high levels of KLF2 and KLF4, showed better colonization of the epiblast than did rbEKA-mid-S_{10}L cells (14%

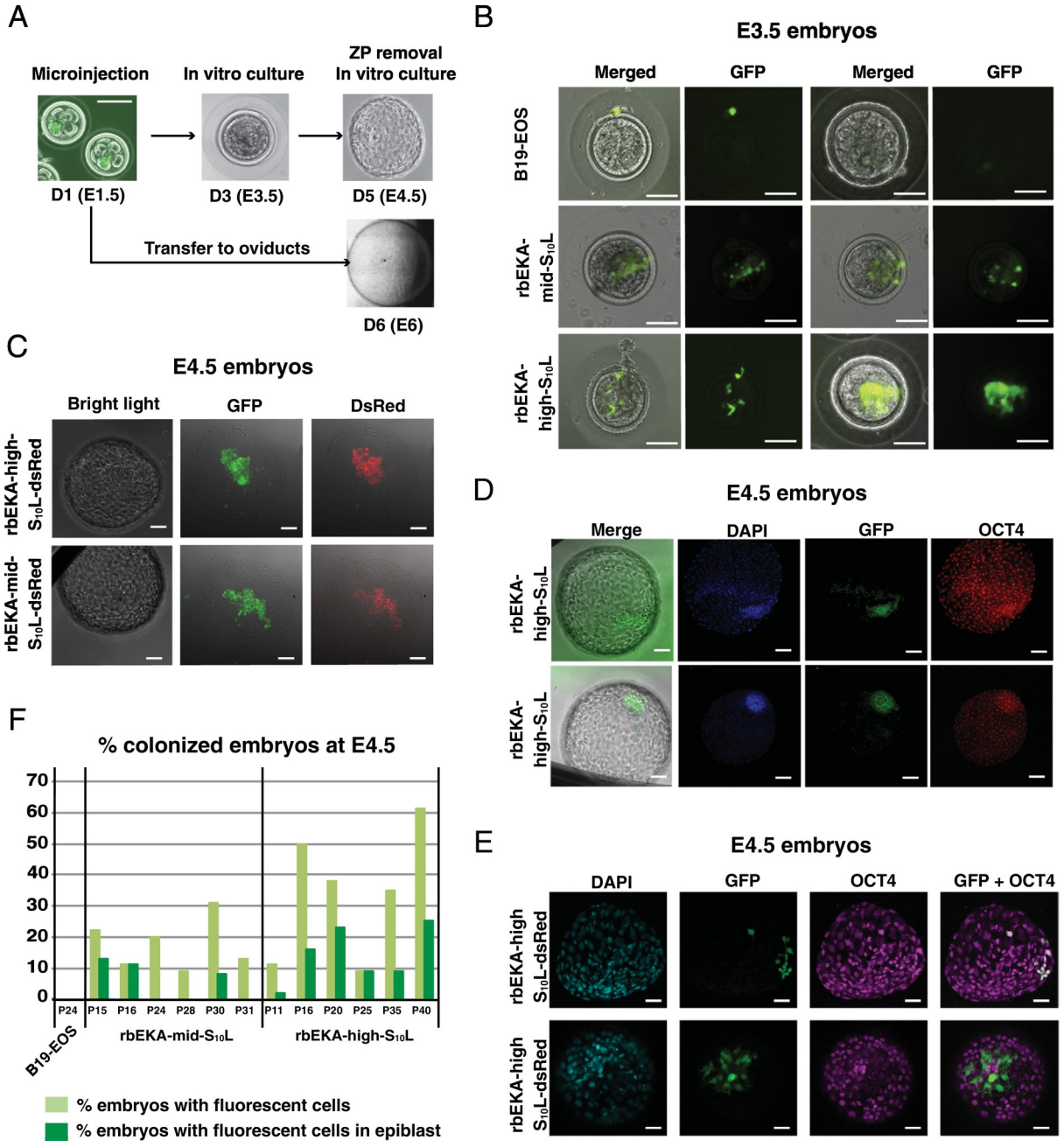

Fig. 6. Integration and survival in the ICM. (A) Strategy used to assess the capacity of rbEKA-S_{10}L cells to colonize rabbit pre-implantation embryos. (B) Phase-contrast and epifluorescence images of the early-blastocyst stage embryos (E3.5) resulting from the microinjection of B19-EOS (P10), rbEKA-mid-S_{10}L (P10), and rbEKA-high-S_{10}L (P10) cells (scale bars = 50 μm). (C–E) Phase-contrast and confocal fluorescence images of the mid-blastocyst stage embryos (E4.5) resulting from the microinjection of rbEKA- S_{10}L cells (scale bars = 50 μm); (C) immunolabeling with anti-GFP antibody; (D,E) Immunolabeling with anti-GFP and anti-Oct4 antibodies. (F) Histogram showing the percentage of E4.5 blastocysts with GFP-positive cells in the epiblast after microinjection of B19-EOS, rbEKA-mid-S_{10}L, and rbEKA-high-S_{10}L cells.

and 7% of the injected embryos, respectively). Double immunolabeling of GFP and Oct4 revealed co-expression of the two markers in the epiblast (Fig. 6D,E). A few embryos displayed large GFP-positive cells outside the epiblast. These cells showed both weak GFP immunostaining and weak Oct4 immunostaining, suggestive of early trophoblast cells (Fig. 6E).

In the third step, we investigated the capability of rbEKA-high-S_{10}L-dsRed cells to colonize the embryonic disk of pre-gastrula and primitive streak embryos. For this, 8-cell stage rabbit embryos were microinjected with 5–10 rbEKA-high-S_{10}L-dsRed cells and were transferred into the oviduct of surrogate mothers. In total, 434 embryos were recovered after 5 days, of which 6 embryos showed colonization of the embryonic disk by GFP-positive cells (Fig. 7A–C, and Supplementary Table S1). Two of them were pooled prior to dissociation to single cells and single-cell qRT-PCR analysis for expression of early and late epiblast markers. Twenty-four cells were analyzed in total, of which five expressed dsRed (Fig. 7D). Four dsRed-positive cells (e1-c4, e1-c8, e2-c3, and e2-c9) co-expressed *Pou5f1*, *Pecam1*, *Nanog*, *Gbx2*, and *Klf17*. Two of them (e2-c3, and e2-c9) showed low levels of *Cdh9*, *Otx2*, *Fgf4*, *Khdc1* transcripts, and high levels of *Cdh1* and *Tfcp2l1* transcripts, similar to their host counterparts. The fifth dsRed-positive cells (e1-c10) clustered with the second group of host cells, which expressed *Pou5f1*, *Pecam1*, *Nanog*, *Gbx2*, and *Klf17* at lower levels than the first group of cells. We speculate that the e1-c10 cell was committed to differentiation.

Finally, 59 fetuses resulting from the injection of rbEKA-S_{10}L-dsRed cells into 8-cell stage embryo (early morula) were recovered at E10.

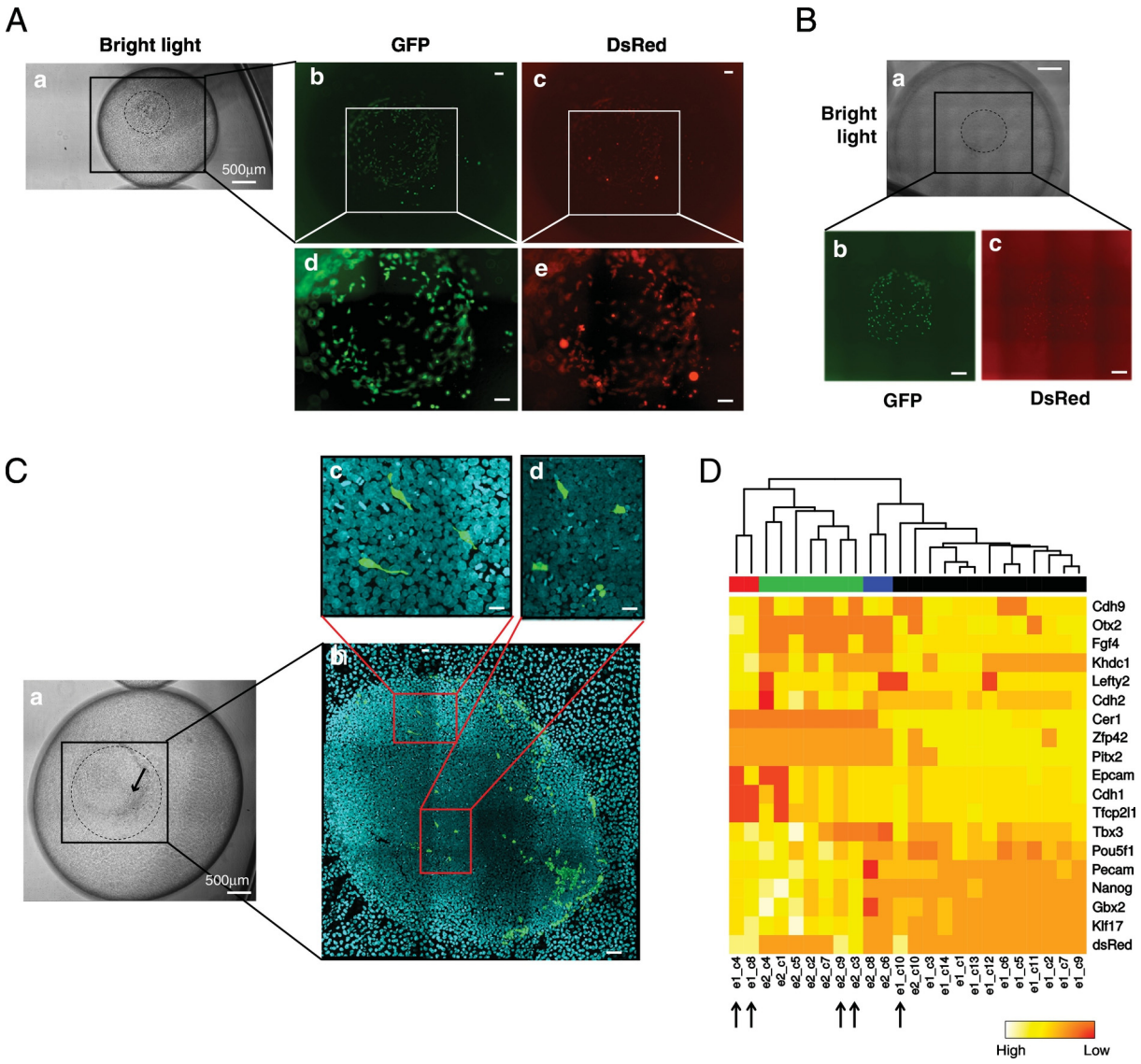

Fig. 7. Epiblast colonization. Phase-contrast and fluorescence images of E6 embryo resulting from the microinjection of rbEKA-high-S_{10}L cells in the 8-cell stage embryos and subsequent transfer into the oviducts of surrogate mothers for 5 days. (A) E6.0 stage 1 embryo (Puschel and Viebahn, 2010); (a) Phase-contrast image (scale bar = 500 µm). (b, c, d, e,) Higher magnification of the E6 embryo showing the embryonic disk in GFP fluorescence (b,d), and dsRed fluorescence (c,e) (Scale bar = 50 µm). (B) E6.2 stage 2 embryo (Puschel and Viebahn, 2010); (a) Phase-contrast image (Scale bar = 500 µm). (b,c) Higher magnification of the E6 embryo showing the GFP and dsRed fluorescence in the embryonic disk (Scale bar = 50 µm). (C) E6.5 stage 3 embryo (Puschel and Viebahn, 2010); (a) Phase-contrast image (Scale bar = 500 µm). Primitive streak is indicated with an arrow. (b,c,d) Higher magnification of the E6.5 embryo showing the GFP fluorescence in the embryonic disk (b, scale bar = 50 µm; c,d: scale bar = 10 µm). (D) Heatmap calculated from single-cell qRT-PCR data. Values displayed correspond to the expression level in each cell adjusted by the mean expression of each gene across samples (explain color scale).

Two fetuses showed dsRed-positive cells in the brain region (Supplementary Fig. S11A, and Supplementary Table S1). To confirm the presence of rbEKA-derived cells, 15 fetuses (out of 59) were analyzed by PCR with genomic DNA and primers encompassing the *Klf2-2A-Klf4* sequence, of which the two with dsRed-positive cells showed the expected 60 nt fragment with the nucleotide sequence encompassing the 2A region (Supplementary Fig. S11B,C). In those two fetuses, the rate of chimerism was evaluated to approximately 1%.

These results demonstrate that the rbEKA-S_{10}L cells colonize the ICM of host embryos and participate in epiblast expansion. However, the rate of chimerism decreased in more advanced embryos, suggesting that the descendants of the rbEKA-S_{10}L cells appeared to be progressively eliminated during embryo development.

4. Discussion

We showed that overexpression of KLF2 and KLF4 and culturing in a medium supplemented with FCS and LIF reconfigured the rbiPSC transcriptome to resemble that of pluripotent cells of the pre-implantation embryo. These results are in line with those of two previous studies in mice and humans. The first study showed that forced expression of Klf4 was sufficient to reprogram mouse FGF2-dependent EpiSCs into germline competent, LIF-dependent mESCs (Guo et al., 2009). The second study showed that overexpression of KLF2 and KLF4, replacement of FGF2 with LIF, and treatment with GSK3β and MEK inhibitors allowed hESCs to acquire genetic and epigenetic characteristics resembling those of mouse cells in the naïve state of pluripotency (Hanna et al., 2010). Similar to converted mESCs and naïve-like hESCs, rabbit rbEKA-S_{10}L cells are permissive to single-cell dissociation with trypsin and express elevated levels of naïve state-specific transcription factors and miRNAs defined in mice. However, rbEKA-S_{10}L cells, unlike converted mESCs, depend on FGF2 and activin signaling, but not on LIF/JAK signaling for self-renewal. Moreover, rbEKA-S_{10}L cells are not permissive to long-term propagation in the presence of two inhibitors, which is a hallmark of ground state pluripotency in rodents (Silva et al., 2008; Ying et

al., 2008), human (Chen et al., 2015a; Guo et al., 2016; Takashima et al., 2014; Theunissen et al., 2014) and cynomolgus monkey (Chen et al., 2015b). When benchmarked against E4-stage ICM and E6-stage epiblast for pluripotency gene expression, the rbEKA-S_{10}L cells clustered closely to the E6-stage epiblast. Together, these results suggest that the rbEKA-S_{10}L cells exhibit characteristic features of both the naïve and primed pluripotency defined in mice. Such an intermediate position raises the question of whether rbEKA-S_{10}L cells have only undergone partial reprogramming to naïve-like pluripotency defined in mice, match naïve pluripotency defined in rabbits, or both. We still cannot answer this question, since we know very little about the molecular signature of naïve pluripotency in rabbit. Klf2 and Klf4 might be necessary but not sufficient to reprogram rabbit iPS cells to bona fide naïve pluripotency. Alternatively, the mere existence of naïve versus primed states of pluripotency in the rabbit embryo is an open question. Interestingly, three markers of naïve pluripotency in mice, *Nr0b1* and *Gbx2*, were more highly expressed in B19-EOS cells compared with rabbit ICM cells, and their expression decreased after reprogramming into rbEKA-S_{10}L cells. Additionally, we failed at quantifying their expression in rabbit ICMs using qPCR, which signifies low expression levels (data not shown). In a mirror image *Otx2*, a marker of primed pluripotency (expressed in mEpiSCs), was highly expressed in rabbit ICM cells, and its expression increased in rbEK-S_{10}L cells compared with B19-EOS cells. These findings suggest that the molecular signature of rabbit ICM cells would differ partially from that of mice ICM cells. Therefore, a thorough characterization of the transcriptome of pluripotent cells in the E4-stage ICM and E6-stage epiblast is essential to identify the defining markers of naïve pluripotency in rabbit.

Despite rbEKA-S_{10}L cells lacking both dependency on LIF/STAT3 signaling and resistance to MEK inhibition, they could survive and incorporate into rabbit ICM and participate in the expansion of the epiblast with a remarkable efficiency. Therefore, unlike rodents, colonization of epiblast after injection of pluripotent stem cells into 8-cell stage embryos is compatible with the use of FGF2/ERK and activin/Smad signaling in rabbits. This is in line with the results of studies on the cynomolgus monkey showing that the naïve-like NHSMV ESCs, which required both FGF2 and TGFβ1 for propagation in the undifferentiated state, efficiently colonized the monkey pre-implantation embryo (Chen et al., 2015b). It is unclear whether the capacity of rbEKA-S_{10}L cells to colonize the epiblast results from the global resetting of transcription factors that forms the naïve pluripotency network or from the activation of limited number of key genes. A previous study showed that mEpiSCs could be incorporated into the mouse ICM after blastocyst injection by forced expression of *Cdh1* transgene, which encodes E-cadherin (Ohtsuka et al., 2012). Interestingly, rbEKA-S_{10}L cells showed a robust activation of *Cdh1*.

We observed that the rate of successfully colonized rabbit embryos decreased from the mid-blastocyst stage to the early gastrula stage. A similar observation could be made in the cynomolgus monkey after injection of naïve-like NHSMV ESCs into morula, where chimeric fetuses at E100 displayed a much lower contribution of the injected cells than did the chimeric blastocysts (Chen et al., 2015b). It is possible that GFP-positive cells observed in the E4 rabbit blastocysts were not truly incorporated into the ICM and only a few of them successfully colonized the epiblast and contributed to its expansion, which is in line with previous observations in mice (Wang and Jaenisch, 2004). Another plausible explanation is a weak competitive edge of rbEKA-S_{10}L cells and their progeny against the host cells in contributing to late epiblast expansion and differentiation. Thus, the generation of postnatal chimeras will require designing PSCs that can successfully compete with host cells within all somatic and germ lineages.

Author contributions

Y.T., M.A., E.G., N.B., V.D., and P.S. conceived and designed the study. Y.T., M.A., I.A., A.M., W.B., L.M., M.A., P.O., J.N-F., I.O., T.J. C.A., N.P., B·S-P. H.B., A.P., J.L., E.G. and N.B. performed the experiments. C.M. and L.J. performed biostatistics analysis. M.A., N.B., V.D. and P.S. wrote the manuscript.

Acknowledgments

This work was supported by research grants from “Agence Nationale de la Recherche” (ANR) (projects PLURABBIT n°PCS-09-GENM-08 & ORYCTOGENE n°ANR-12-RPIB-0013), the European Cooperation in Science and Technology (COST) Action (Rabbit Genome Biology (RGB)-Net n°TD1101), the HyPharm Company, the “Région Rhône-Alpes” (ADR CIBLE 2010 project n°R10065CC to Y.T.), the Infrastructure Nationale en Biologie et Santé INGESTEM (ANR-11-INBS-0009), the Infrastructure Nationale en Biologie et Santé CRB-Anim (ANR-11-INBS-0003), the IHU-B CESAME (ANR-10-IBHU-003), and the LabEx “DEVweCAN” (ANR-10-LABX-0061), the LabEx "CORTEX" (ANR-11-LABX-0042) of the University of Lyon within the program ‘Investissements d'Avenir’ (ANR-11-IDEX-0007).

Appendix A. Supplementary data

Supplementary data to this article can be found online at http://dx.doi.org/10.1016/j.scr.2017.09.001.

References

Bao, S., Tang, F., Li, X., Hayashi, K., Gillich, A., Lao, K., Surani, M.A., 2009. Epigenetic reversion of post-implantation epiblast to pluripotent embryonic stem cells. Nature 461, 1292–1295.

Besenfelder, U., Strouhal, C., Brem, G., 1998. A method for endoscopic embryo collection and transfer in the rabbit. Zentralblatt fur Veterinarmedizin Reihe A 45, 577–579.

Boroviak, T., Loos, R., Bertone, P., Smith, A., Nichols, J., 2014. The ability of inner-cell-mass cells to self-renew as embryonic stem cells is acquired following epiblast specification. Nat. Cell Biol. 16, 516–528.

Boroviak, T., Loos, R., Lombard, P., Okahara, J., Behr, R., Sasaki, E., Nichols, J., Smith, A., Bertone, P., 2015. Lineage-specific profiling delineates the emergence and progression of naive pluripotency in mammalian embryogenesis. Dev. Cell 35, 366–382.

Brons, I.G., Smithers, L.E., Trotter, M.W., Rugg-Gunn, P., Sun, B., Chuva de Sousa Lopes, S.M., Howlett, S.K., Clarkson, A., Ahrlund-Richter, L., Pedersen, R.A., et al., 2007. Derivation of pluripotent epiblast stem cells from mammalian embryos. Nature 448, 191–195.

Chan, Y.S., Goke, J., Ng, J.H., Lu, X., Gonzales, K.A., Tan, C.P., Tng, W.Q., Hong, Z.Z., Lim, Y.S., Ng, H.H., 2013. Induction of a human pluripotent state with distinct regulatory circuitry that resembles preimplantation epiblast. Cell Stem Cell 13, 663–675.

Chen, H., Aksoy, I., Gonnot, F., Osteil, P., Aubry, M., Hamela, C., Rognard, C., Hochard, A., Voisin, S., Fontaine, E., et al., 2015a. Reinforcement of STAT3 activity reprogrammes human embryonic stem cells to naïve-like pluripotency. Nat. Commun. 6, 7095–7112.

Chen, Y., Niu, Y., Li, Y., Ai, Z., Kang, Y., Shi, H., Xiang, Z., Yang, Z., Tan, T., Si, W., et al., 2015b. Generation of Cynomolgus monkey chimeric fetuses using embryonic stem cells. Cell Stem Cell 17, 116–124.

Gafni, O., Weinberger, L., Mansour, A.A., Manor, Y.S., Chomsky, E., Ben-Yosef, D., Kalma, Y., Viukov, S., Maza, I., Zviran, A., et al., 2013. Derivation of novel human ground state naive pluripotent stem cells. Nature 504, 282–286.

Guo, G., Smith, A., 2010. A genome-wide screen in EpiSCs identifies Nr5a nuclear receptors as potent inducers of ground state pluripotency. Development 137, 3185–3192.

Guo, G., Yang, J., Nichols, J., Hall, J.S., Eyres, I., Mansfield, W., Smith, A., 2009. Klf4 reverts developmentally programmed restriction of ground state pluripotency. Development 136, 1063–1069.

Guo, G., von Meyenn, F., Santos, F., Chen, Y., Reik, W., Bertone, P., Smith, A., Nichols, J., 2016. Naive pluripotent stem cells derived directly from isolated cells of the human inner cell mass. Stem cell reports 6, 437–446.

Hall, J., Guo, G., Wray, J., Eyres, I., Nichols, J., Grotewold, L., Morfopoulou, S., Humphreys, P., Mansfield, W., Walker, R., et al., 2009. Oct4 and LIF/Stat3 additively induce Kruppel factors to sustain embryonic stem cell self-renewal. Cell Stem Cell 5, 597–609.

Hanna, J., Cheng, A.W., Saha, K., Kim, J., Lengner, C.J., Soldner, F., Cassady, J.P., Muffat, J., Carey, B.W., Jaenisch, R., 2010. Human embryonic stem cells with biological and epigenetic characteristics similar to those of mouse ESCs. Proc. Natl. Acad. Sci. U. S. A. 107, 9222–9227.

Honda, A., Hirose, M., Ogura, A., 2009. Basic FGF and Activin/nodal but not LIF signaling sustain undifferentiated status of rabbit embryonic stem cells. Exp. Cell Res. 315, 2033–2042.

Hotta, A., Cheung, A.Y., Farra, N., Vijayaragavan, K., Seguin, C.A., Draper, J.S., Pasceri, P., Maksakova, I.A., Mager, D.L., Rossant, J., et al., 2009. Isolation of human iPS cells using EOS lentiviral vectors to select for pluripotency. Nat. Methods 6, 370–376.

Illich, D.J., Zhang, M., Ursu, A., Osorno, R., Kim, K.P., Yoon, J., Arauzo-Bravo, M.J., Wu, G., Esch, D., Sabour, D., et al., 2016. Distinct signaling requirements for the establishment of ESC pluripotency in late-stage EpiSCs. Cell Rep. 15, 787–800.

Jacquier, V., Estelle, J., Schmaltz-Panneau, B., Lecardonnel, J., Moroldo, M., Lemonnier, G., Turner-Maier, J., Duranthon, V., Oswald, I.P., Gidenne, T., et al., 2015. Genome-wide immunity studies in the rabbit: transcriptome variations in peripheral blood mononuclear cells after in vitro stimulation by LPS or PMA-Ionomycin. BMC Genomics 16, 26.

Maraghechi, P., Hiripi, L., Toth, G., Bontovics, B., Bosze, Z., Gocza, E., 2013. Discovery of pluripotency associated microRNAs in rabbit preimplantation embryos and embryonic stem-like cells. Reproduction 145, 421–437.

Nichols, J., Smith, A., 2009. Naive and primed pluripotent states. Cell Stem Cell 4, 487–492.

Ohtsuka, S., Nishikawa-Torikai, S., Niwa, H., 2012. E-cadherin promotes incorporation of mouse epiblast stem cells into normal development. PLoS One 7, e45220.

Osteil, P., Tapponnier, Y., Markossian, S., Godet, M., Schmaltz-Panneau, B., Jouneau, L., Cabau, C., Joly, T., Blachere, T., Gocza, E., et al., 2013. Induced pluripotent stem cells derived from rabbits exhibit some characteristics of naive pluripotency. Biol. Open. 2, 613–628.

Osteil, P., Moulin, A., Santamaria, C., Joly, T., Jouneau, L., Aubry, M., Tapponnier, Y., Archilla, C., Schmaltz-Panneau, B., Lecardonnel, J., et al., 2016. A panel of embryonic stem cell lines reveals the variety and dynamic of pluripotent states in rabbits. Stem cell reports 7, 383–398.

Puschel, B., Viebahn, C., 2010. Rabbit Mating and Embryo Isolation. Cold Spring Harbor Protocols 2010 pdb prot5350.

Schmaltz-Panneau, B., Jouneau, L., Osteil, P., Tapponnier, Y., Afanassieff, M., Moroldo, M., Jouneau, A., Daniel, N., Archilla, C., Savatier, P., et al., 2014. Contrasting transcriptome landscapes of rabbit pluripotent stem cells in vitro and in vivo. Anim. Reprod. Sci. 149, 67–79.

Silva, J., Barrandon, O., Nichols, J., Kawaguchi, J., Theunissen, T.W., Smith, A., 2008. Promotion of reprogramming to ground state pluripotency by signal inhibition. PLoS Biol. 6, e253.

Silva, J., Nichols, J., Theunissen, T.W., Guo, G., van Oosten, A.L., Barrandon, O., Wray, J., Yamanaka, S., Chambers, I., Smith, A., 2009. Nanog is the gateway to the pluripotent ground state. Cell 138, 722–737.

Smith, Z.D., Sindhu, C., Meissner, A., 2016. Molecular features of cellular reprogramming and development. Nat. Rev. Mol. Cell Biol. 17, 139–154.

Tachibana, M., Sparman, M., Ramsey, C., Ma, H., Lee, H.S., Penedo, M.C., Mitalipov, S., 2012. Generation of chimeric rhesus monkeys. Cell 148, 285–295.

Takashima, Y., Guo, G., Loos, R., Nichols, J., Ficz, G., Krueger, F., Oxley, D., Santos, F., Clarke, J., Mansfield, W., et al., 2014. Resetting transcription factor control circuitry toward ground-state pluripotency in human. Cell 158, 1254–1269.

Tang, F., Barbacioru, C., Bao, S., Lee, C., Nordman, E., Wang, X., Lao, K., Surani, M.A., 2010. Tracing the derivation of embryonic stem cells from the inner cell mass by single-cell RNA-Seq analysis. Cell Stem Cell 6, 468–478.

Tesar, P.J., Chenoweth, J.G., Brook, F.A., Davies, T.J., Evans, E.P., Mack, D.L., Gardner, R.L., McKay, R.D., 2007. New cell lines from mouse epiblast share defining features with human embryonic stem cells. Nature 448, 196–199.

Theunissen, T.W., Powell, B.E., Wang, H., Mitalipova, M., Faddah, D.A., Reddy, J., Fan, Z.P., Maetzel, D., Ganz, K., Shi, L., et al., 2014. Systematic identification of culture conditions for induction and maintenance of naive human pluripotency. Cell Stem Cell 15, 471–487.

Vallier, L., Alexander, M., Pedersen, R.A., 2005. Activin/nodal and FGF pathways cooperate to maintain pluripotency of human embryonic stem cells. J. Cell Sci. 118, 4495–4509.

Wang, Z., Jaenisch, R., 2004. At most three ES cells contribute to the somatic lineages of chimeric mice and of mice produced by ES-tetraploid complementation. Dev. Biol. 275, 192–201.

Wang, S., Tang, X., Niu, Y., Chen, H., Li, B., Li, T., Zhang, X., Hu, Z., Ji, W., 2006. Generation and characterization of rabbit embryonic stem cells. Stem Cells 25, 481–489.

Wang, S., Shen, Y., Yuan, X., Chen, K., Guo, X., Chen, Y., Niu, Y., Li, J., Xu, R.H., Yan, X., et al., 2008. Dissecting signaling pathways that govern self-renewal of rabbit embryonic stem cells. J. Biol. Chem. 19, 35929–35940.

Wianny, F., Bernat, A., Marcy, G., Huissoud, C., Markossian, S., Leviel, V., Kennedy, H., Savatier, P., Dehay, C., 2008. Derivation and cloning of a novel rhesus ES cell line stably expressing tau-GFP. Stem Cells 26, 1444–1453.

Yang, J., van Oosten, A.L., Theunissen, T.W., Guo, G., Silva, J.C., Smith, A., 2010. Stat3 Activation is limiting for reprogramming to ground state pluripotency. Cell Stem Cell 7, 319–328.

Yeom, Y.I., Fuhrmann, G., Ovitt, C.E., Brehm, A., Ohbo, K., Gross, M., Hubner, K., Scholer, H.R., 1996. Germline regulatory element of Oct-4 specific for the totipotent cycle of embryonal cells. Development 122, 881–894.

Ying, Q.L., Wray, J., Nichols, J., Batlle-Morera, L., Doble, B., Woodgett, J., Cohen, P., Smith, A., 2008. The ground state of embryonic stem cell self-renewal. Nature 453, 519–523.